DISCRETE ELEMENT MODELLING OF THE FRESH STATE BEHAVIOR OF PERVIOUS CONCRETE

AUTHORS

R. Pieralisi [a, *], S. H. P. Cavalaro [a, *], A. Aguado [a]

[a] Departamento de Ingeniería Civil y Ambiental, E.T.S. Ingenieros de Caminos, Canales y Puertos, Universidad Politécnica de Cataluña, BarcelonaTech, Jordi Girona Salgado 1-3, Módulo C1, Despacho 202, 08034 Barcelona, Spain

CORRESPONDING AUTHOR

[*] Tel.: +34 934054247; fax: +34 934054135.

E-mail address: ricardo.pieralisi@upc.edu; sergio.pialarissi@upc.edu

ABSTRACT

The objective of this paper is to propose a novel numerical approach to model the compaction process of pervious concrete in the fresh state, taking into account input parameters related with the mix composition. A new constitutive model applied to Discrete Element Method was developed for the simulation of the interaction between aggregates connected by fresh cement paste. This approach reproduces the velocity dependency of the fresh cement paste. A calibration was conducted with data from the literature. Furthermore, an extensive experimental program considering different shapes of aggregates, grading curves and aggregate-to-cement paste ratios was performed to evaluate the fresh state behavior and validate the numerical models. The good fit obtained between numerical and experimental results confirm the model and the constitutive law

reproduce the under uniaxial compaction, thus representing a step forward in the design and application of pervious concrete mixes.

KEYWORDS

Pervious Concrete; Fresh Cement Paste; Discrete Element Model; Compaction; Constitutive Law

1. INTRODUCTION

Pervious concrete is a material that combines adequate mechanical properties and high permeability [1-4]. These properties are governed by the mix composition and, especially, the compaction process applied to the material in the fresh state. In terms of mix composition, the traditional philosophy used to achieve a pervious concrete is to reduce the amount of fines provided by the sand and to use cement paste contents just enough to create a connection between coarse aggregates. The fresh state mixture obtained may be dissociated in several unities. Each unity is composed by an aggregate involved by a thin layer of dry cement paste obtained by using low water-to-cement ratios or special thickening admixtures. The low fluidity achieved is a key point that helps to reduce the risk of segregation of the mixture.

The bulk material obtained after mixing usually has a porosity around 50 % by volume. On the other hand, values ranging from 15 % to 30 % [5-7] are commonly found in the final application after the compaction process. It is evident that a significant reduction on the porosity occurs in the compaction process, which plays a fundamental role on the performance of the material [8-10] since bigger porosities increase the drainage capacity but compromise the mechanical strength.

In general, the evaluation of the compaction process and of the final porosity of pervious concrete is performed experimentally through a trial and error approach according with a time-consuming process. The assessment of the fresh state behavior of the material and the compaction using numerical simulations is still a relatively unexplored field.

The discrete element method (DEM) [11-13] is a powerful tool capable of simulating the dynamic movement and the interaction of a large number of particles found in granular materials. Particles are assumed as spherical bodies that may have contact

with each other. Traditionally, a linear elastic contact approximation is used to simulate interactions, considering that an overlap is possible between two particles at the points of contact. This overlap generates forces of interaction governed by a constitutive law.

Several authors have simulated the fresh state behavior of concrete using DEM. Almost all of them focus on highly flowable concrete (self-compacting). Nabeta [14] introduced the simulations of fresh concretes flow using DEM. Chu *et al.* [15] used DEM to simulate the filling capacity of fresh concrete. The authors considered a homogenous material approach in which all particles share the same properties. Afterwards, other studies [16-17] introduced a heterogeneous approach, using some particles to simulate the aggregates and others to simulate the cement paste or mortar. Nevertheless, with the advances in processing capabilities of modern computers, it becomes possible to use models with elevated complexity. A recent approach to simulate the flow of self-compacting concrete was proposed by Chu *et al.* [18]. In the latter, a bi-phasic particle with an aggregate-like kernel involved by a mortar layer was used to simplify the computation of interactions. In a similar way, Zheng *et al.* [19] proposed a GPU-based parallel algorithm for particle contact detection in self-compacting fresh concrete simulations.

In order to simulate the fresh state properties of self-compacting concrete, Gram [20] proposed an adaptation of the Bingham contact using a spring connected in parallel with a serial connection of a damper and a Saint-Venant element. Other authors [21-24] have proposed contact models based on stress-strain (σ-ε) curves obtained with laboratory tests in which two spheres surrounded by mortar or cement paste are put in contact. In another study, Remond *et al.* [25] proposed a bi-phasic model with the simulation of a fluid-like interaction between the external layers of the particles. Roussel *et al.* [26] compared several numerical techniques (DEM, Computational Fluid Dynamics and

Lattice Boltzman) for the simulation of the concrete flow. In their work [26], the authors suggested that all these numerical techniques have reached a level that allows simulating practical problems.

Despite the advances observed, it is important to remark that the great majority of the studies with DEM focuses on self-compacting concrete with a high fluidity and without accounting for external compaction or vibration. On the contrary, scarce information about the evaluation of the fresh state properties of pervious concrete may be found, especially regarding the simulation of the compaction process.

The objective of this study is to propose and validate a DEM approach for the simulation of the compaction process of pervious concrete in fresh state. In this sense, it is necessary to propose a constitutive law that represents the interaction of two particles (or aggregates) surrounded by a thin layer of cement paste in fresh state. A biphasic particle and a new constitutive law for the interactions between particles more representative with pervious concretes were proposed and implemented in the open source framework YADE [27].

A calibration of the constitutive law with the experimental results from Shyshko *et al.* [21] was performed and an experimental program related to the compaction process of the pervious concrete in fresh state was conducted. In this experimental program, 3 different types of aggregates and 4 aggregate-to-cement paste ratio were tested. The good fit obtained between numerical and experimental results confirm the model and the constitutive law reproduce the fresh state behavior of the pervious concrete under uniaxial compaction. The results obtained represent a step forward, showing that it is possible to apply advanced numerical tools for a preliminary assessment of the performance of pervious concrete, which might have positive implications in the design and use of mixes in the future.

2. EXPERIMENTAL PROGRAM

The experimental program was divided in two phases. Phase I focused on the effect of the cement paste-to-aggregate ratio (P/A) in mixes with regular mono-sized particles. Phase II was centered on the effect of the type and grading of the aggregates.

2.1. Materials Properties

In Phase I, spherical glass aggregates (see Fig. 1a) with diameter of 18 ± 0.5 mm and density of 2570 kg/m^3 was used. In Phase II, crushed limestone with density of 2640 kg/m^3 and water absorption of 0.83% by weight was used. The crushed limestone aggregates were sieved to ensure that particle sizes were between 5 and 12 mm (see Fig. 1b) and between 9 to 20 mm (see Fig. 1c). In order to maximize the porosity achieved, after the sieving process, the aggregates were washed to eliminate remaining limestone dust. The grading curves and the properties of the aggregates are presented in Fig. 1d. The cement used all mixes was CEM II/A-L 42.5R.

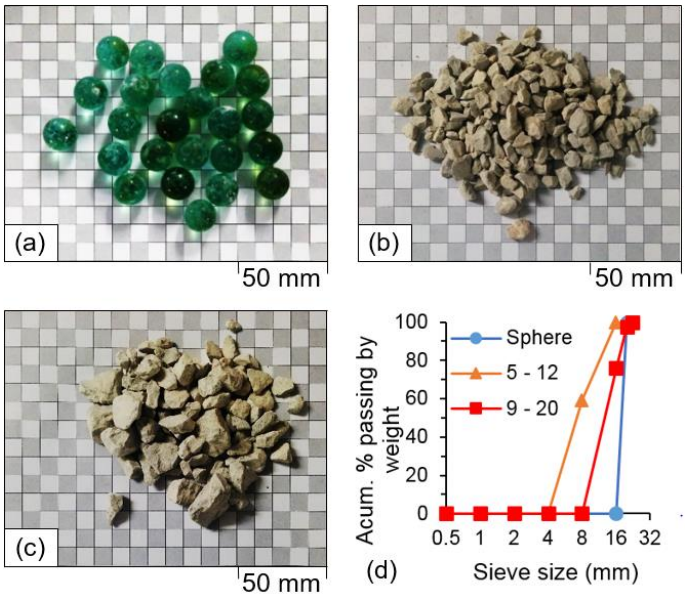

Figure 1 – Surficial aspect of spherical glasses (a), limestone from 5/12 (b), limestone 9/20 (c) and the grading curves (d)

2.2. Compositions

The compositions used in the experimental program were defined to simulate those found in typical applications of pervious concrete. All compositions had a fixed theoretical content of aggregates equal to 1400 kg/m^3. The water-to-cement ratio (w/c) was also the same for all mixes in order to guarantee that the cement pastes obtained had similar rheology. Moreover, 1 % of retardant by cement weight was added in order to diminish variations in the fresh state properties of the concrete during the compaction of the specimens.

The content of cement was defined depending on the type of aggregate. In the case of mixes from Phase I, contents of cement equal to 215, 245, 275 and 305 kg/m^3 were used. The cement paste-to-aggregate ratio (P/A) by weight ranged from 0.15 to 0.22, approximately. Mixes from phase II had a theoretical content of cement set at 400 kg/m^3, equivalent to a P/A of 0.29.

The variations in terms of the content of cement between mixes from Phases I and II are a consequence of the difference in the specific surface of the aggregates, which affects the total surface that has to be involved by the cement paste. The low specific surface of the mono-sized glass spheres from Phase I is involved by a smaller amount of paste, leading to smaller cement content and smaller P/A. On the contrary, in the case of limestone aggregates from Phase II, the irregular shape of particles leads to a higher specific surface that requires an additional amount of paste (bigger cement content and P/A ratios). Notice that this does not compromise the evaluation of the numerical models since the amount of aggregates and paste are taken into account in the simulations.

The composition of all mixes are summarized in Tab. 1. The nomenclature adopted to make reference to each mix includes a first letter that indicates the type of aggregate

(G for glass, Ca for limestone with grading from 5 mm to 12 mm and Cb for limestone with grading from 9 mm to 20 mm), followed by the P/A value.

Table 1 – Compositions.

Phase	Ref.	Aggregate			Cement (kg/m^3)	w/c	P/A
		Type	Grading (mm)	Content (kg/m^3)			
I	G0.15	Glass sphere	18	1400	215	0.27	0.15
	G0.17				245		0.17
	G0.20				275		0.20
	G0.22				305		0.22
II	Ca0.29	Lime-stone	5-12	1400	400		0.29
	Cb0.29		9-20		400		0.29

2.3. Mixing Process

The pervious concrete was prepared in a planetary mortar mixer type 65/2 K-3, using a 65 l container. Paddle rotation and planetary speed were 150 and 40 rpm, respectively. First, cement and aggregates were mixed during 60 s. Then, 70 % of the total water was added and mixed during additional 30 s. Finally, the rest of the water and the retardant was added and mixed during additional 60 s.

Once the fresh pervious concrete was mixed, it was immediately placed into a cylindrical mold (with height equals to 200 mm and diameter equal to 100 mm) in three layers. After the mold was filled, the excess of material surpassing the top of the mold was removed to ensure that the initial height of all specimens was 200 mm. The pouring process and the removal was performed with care to avoid introducing compaction forces. The weight of each sample was measured to achieve comparable levels of fresh density.

2.4. Test Method

The press used in this study to evaluate the compaction pressure curve was a "Ibertest Autotest-200/10" with a load cell of maximum 10 kN and 1 % of accuracy, operating in displacement controlled mode with a velocity equal to 3.33×10^{-4} m/s (20 mm/min). A compaction cylinder with a diameter of 95 mm and a height of 65 mm was fixed to the load cell at the top of the press, as depicted in Fig. 2. The specimen (mold filled with the pervious concrete in fresh state) was positioned between the compaction cylinder and the piston of the press. During the test, the piston moved with a constant displacement rate in the axial direction, thus producing the compaction of the specimen.

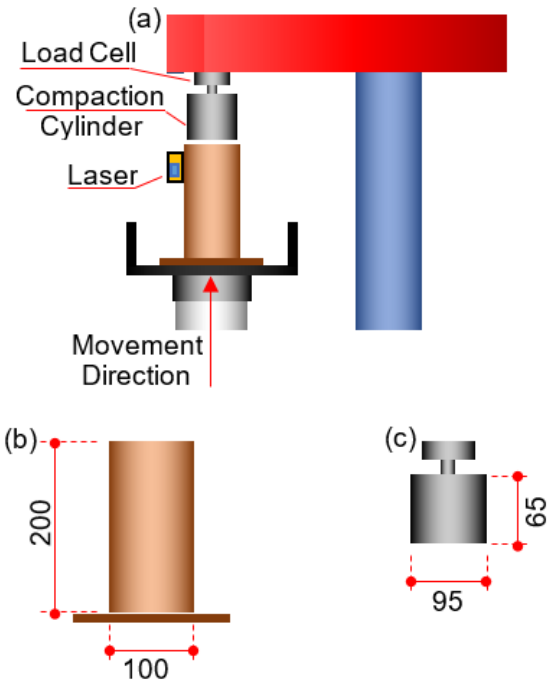

Figure 2 – Test setup (a), mold (b) and compaction cylinder (c) dimensions.

A laser displacement sensor was equipped on the mold wall in order to measure the distance between the top of the mold and the bottom of the compaction cylinder. The data of the displacement and the load measured by the load cell were transmitted to a data acquisition system every 0.2 s. According to the convention adopted, a minimum initial load level of 0.0127 MPa was used to establish the beginning of the measurement. Such

procedure is necessary to homogenize the initial point of the load-strain curve since small variations in the top particles could lead to significant variations in the first stretch of the curves. By fixing a minimum pre-load, the initial condition in terms of distribution of contact with the compaction cylinder becomes similar among all specimens. The test was stopped when the maximum load of 10 kN or the maximum displacement of 40 mm was reached.

The load was divided by the theoretical cross-section of the specimen to estimate the average stress applied. The displacement measured after the pre-load is divided by the original height of the specimen to estimate the strain applied. A stress-strain curve was obtained after the test.

3. EXPERIMENTAL RESULTS AND DISCUSSION

3.1. Phase I

Samples had an average initial mass of 2.02 kg with a standard deviation of 0.07 kg. The estimated initial porosity was approximately 50%. During the compaction process, the specimen undergoes a sudden internal rearrangement due to the high sphericity, low roughness and mono-size of the glass aggregates. This abrupt rearrangement is mainly related to the small number of contacts between each particle and the surrounding ones, which is typical in systems composed by mono-sized unities.

The small number of contacts increases the likelihood of finding casi-unstable or ill-conditioned particles in the system. If sufficient load is applied, these particles may move, changing the support condition of the near particles that also have to move to reach a new stable position. This triggers a chain reaction characterized by a sequential movement in the system.

Such chain reaction produces an abrupt reduction of the load due to the automatic compensation provided by the displacement control from the press. This phenomenon should be more likely to occur in the beginning of the test, which is consistent with the results obtained in Phase I. In order to mitigate the influence of the abrupt load reduction and allow a better comparison with the results from the models, the curve obtained from the compaction process should be filtered. In this sense, only the points with an increment of stress were represented.

Fig. 3a, 3b, 3c and 3d shows compaction curves of the specimens of the families G0.15, G0.17, G0.20 and G0.22, respectively. The curves are characterized by a first stretch where significant increase in the strain is accompanied by small load increments. This is the consequence of the high particle rearrangement experienced in due to the small number of contacts between particles and the big space left in the system (notice that almost 50% by volume of the sample is formed by voids in the beginning of the test). The strain observed is the result of the relative displacement between particles.

After a certain strain takes place, a significant increase in the load is observed for small increments of strain. This is the consequence of the absence of space for the rearrangement of the system and the increase in the number of contacts. In this final part of the curve, the strain is the result of small movements between particles and the deformation of the cement paste layer located around them.

Fig. 3.e shows all curves obtained with glass spheres. The results of the compaction process show a high scatter. Although the identification of a clear trend is difficult, the influence of the P/A seems small in the initial part of the compaction curve. Such outcome was expected since the first stretch of the curve is governed mainly by the rearrangement of the particles with little influence of the thickness of the cement paste layer around the aggregate. The increase of the P/A ratio should increase the thickness of this layer,

affecting the slope of the final stretch of the compaction curve. No clear influence of the P/A ratio is observed in this stretch possibly due to the high scatter of the results.

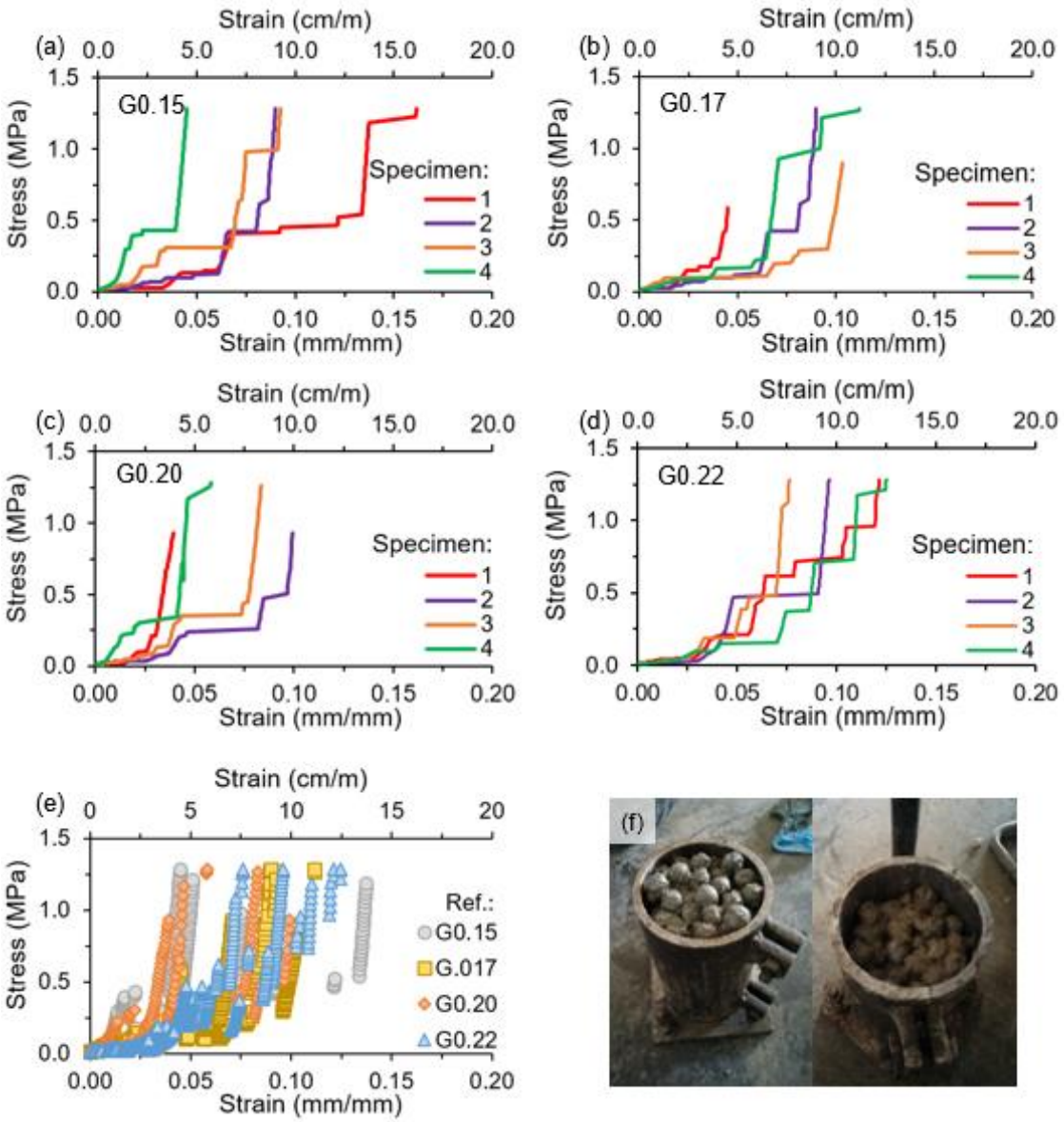

Figure 3 – Measured stress-strain curves (a to e) and image of the specimen before and after the test (f).

3.2. Phase II

Fig. 4a and 4b present the results of concrete Ca0.29 and Cb0.29 with limestone aggregates, respectively. These mixes did not show the abrupt load drop observed in mixes with glass spheres. This is possibly due to the irregular shape, higher surface roughness and varied dimensions of the particles of the limestone aggregates. These

conditions contribute to a bigger number of contact between particles, diminishes the level of rearrangement allowed in the system and limits abrupt movements. Interestingly, a smaller scatter in the results is observed in comparison with those from Phase I (see Fig. 3).

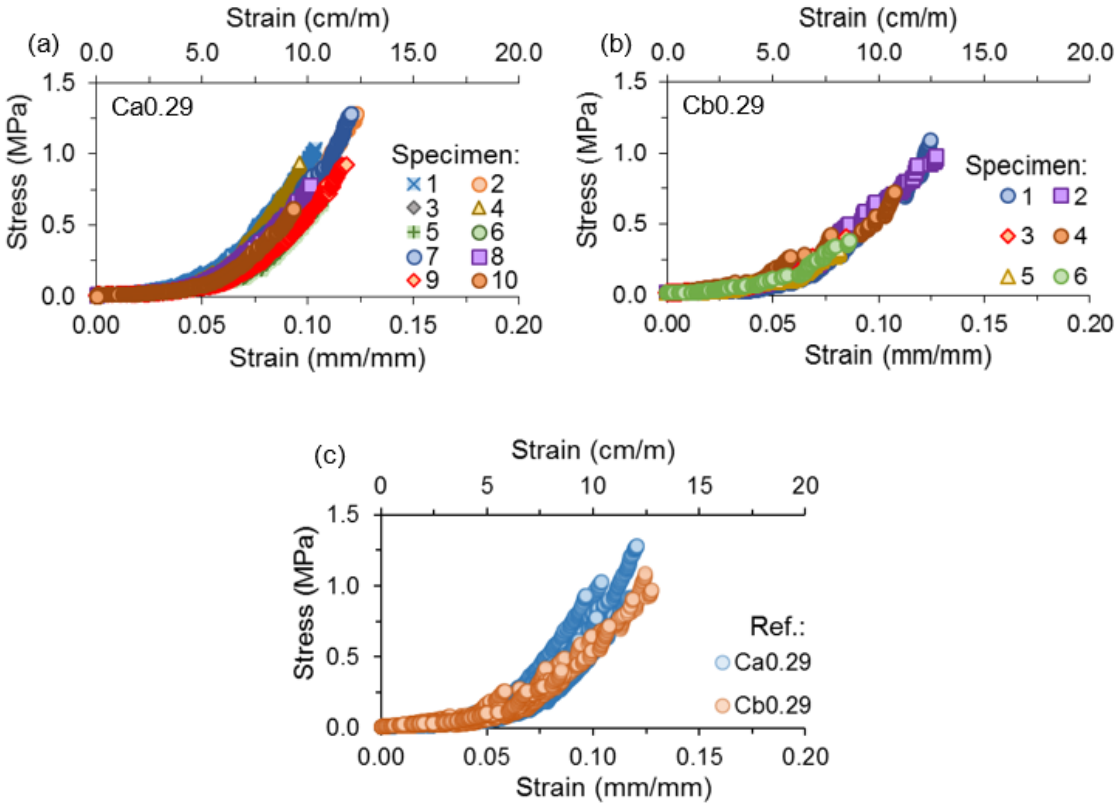

Figure 4 – Measured stress-strain curves of mixes L400a and L400b.

Fig. 4c shows the stress-strain curves of all specimens Ca0.29 and Cb0.29. Notice that the initial stretches of the curves are similar regardless of the change in the nominal size of the aggregate. Conversely, in the final stretch of the curve, the average pressure needed to compact the specimens from Cb0.29 is lower than the average pressure from Ca0.29.

This outcome is also related to the number of contacts between particles. When smaller aggregates are used, more particles are necessary to fill the space, thus generating a bigger number of contacts in the system. This enhances the restriction to internal

rearrangement of the particles. Consequently, as the strain increases, more pressure is needed to achieve higher degrees of compaction.

4. PROPOSAL OF CONSTITUTIVE MODEL

4.1. Particle Definition

The pervious concrete may be dissociated in several unities with the aspect shown in Fig. 5a. Although more complex arrangements are also possible to simulate the real shape, a bi-phasic spherical particle shown in Fig. 5b may be used. The latter has a total radius R_T, being formed by an inner aggregate core with radio R_{ag} surrounded by a paste layer with thickness t_{eq}. The main advantage of this simplification is the low computational cost required to evaluate the contact, as the overlap of spheres is determined from the spatial distance of their centroids without the need to consider their orientation.

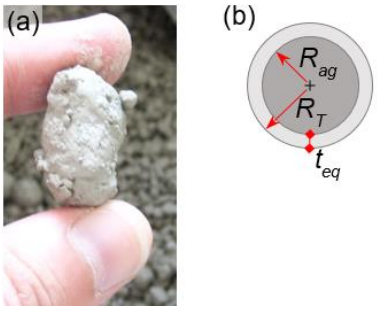

Figure 5 – Real particle formed by aggregate involved by cement paste layer in a pervious concrete (a) and simplification considered (b)

To simulate the open grading curve of the aggregates it is also necessary to define the sizes of particles that will be used in the discretization. As an example, Fig. 6a presents the real grading curve of a coarse aggregate that ranges from 2 to 8 mm, showing the volume that passes through the sieves in the vertical axis and the opening of the sieves in millimeters in the horizontal axis. In this example, an approximation with three different

sizes of aggregate particles (diameters of 2, 4 and 8 mm) was chosen. Through a balance of masses, the percentage of particles corresponding to each size may be calculated, giving the proportion shown in Fig. 6b.

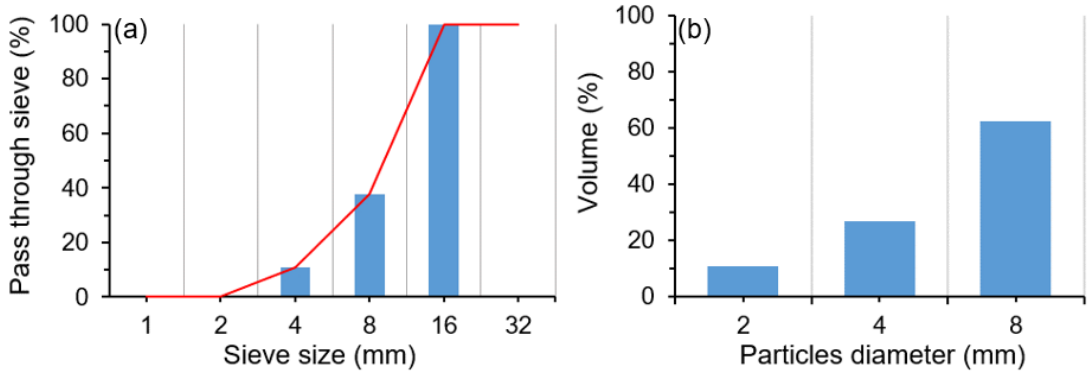

Figure 6 – Approximation of a grading curve with three sizes of aggregate particles (a) and percentage of aggregate particles of each diameter (b)

After the definition of the particles sizes, the thickness of the external layer (t_{eq}) may be calculated. Based on the studies by Klein *et al.* [28], it is considered that t_{eq} is proportional to the radius of the aggregate according with Eq. 1. In this equation, α_{eq} is a constant that accounts for the distribution of the cement paste (or mortar) and depends on the composition of the pervious concrete. In order for Eq. 1 to hold, α_{eq} should be estimated through Eq. 2 with the volume of aggregates (V_{ag}) and the volume cement paste or mortar (V_p) used in the mix. Since the simulations of the pervious concrete are based on the meso-level criteria, the minimal diameter of aggregate should be bigger than the minimal thickness of the cement paste layer. This is always guaranteed with Eq. 1.

$$t_{eq} = R_{ag} \cdot \left(1 + \alpha_{eq}\right) - R_{ag} \tag{1}$$

$$\alpha_{eq} = 1 - \sqrt[3]{1 - \frac{V_p}{V_{ag}}} \tag{2}$$

4.2. Characteristic of the Contact

In the DEM, the particles may interact with each other or with predefined surfaces such as the walls of the molds or of the formwork. The former is known as sphere-sphere (s-s) contact and the latter is known as sphere-wall (s-w) contact, both of which are governed by force-displacement laws.

Considering the definition of the particle previously discussed, the first contact occurs with the viscous mortar or paste external layer surrounding the aggregate. As the overlap increases, the aggregates push the surrounding layer away from the point of contact, causing a lateral volume increase and the formation of a contact bridge (CB). A meniscus-like arrangement depicted in Fig. 7a appears and the mortar or paste thickness separating the aggregate cores or the aggregate core and the wall reduces. Once the initial thickness is consumed, a direct contact is established between aggregates or with the walls.

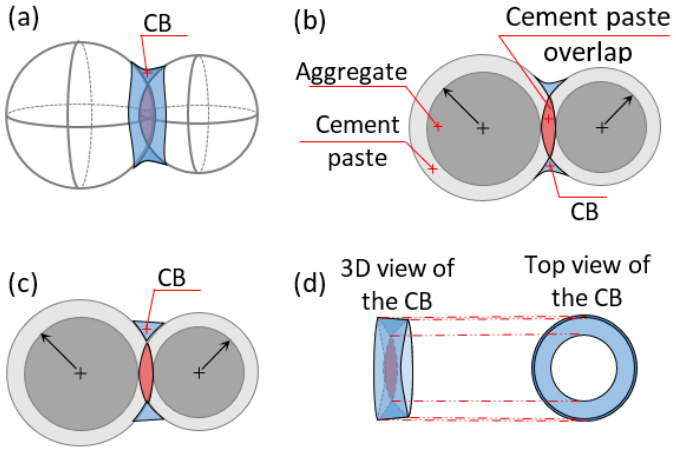

Figure 7 – Formation (a-b) and approximation (c-d) of the CB.

Although the exact simulation of the paste or mortar rearrangement around the aggregate may be performed, it comes with a high computational cost. To mitigate this drawback, the geometrical consideration illustrated in Fig. 7c and 7d was assumed. In line

with the results obtained by Klein *et al.* [29], it is assumed the surface tension of very dry cement paste or mortar is close to 0, which leads to the formation of an almost straight meniscus. In this context, a straight linear average surface is considered a fair approximation of the real situation.

An important geometrical parameter of the contact is the overlapped volume. This is related with the force to produce an approximation of the particles. It is expected that the rearrangement of a bigger volume of paste would require the application of bigger forces. The overlapped volume of the s-s and s-w interactions may be obtained through Eq. 3 and 4, respectively. In these equations, d_i and d_j are the distance between the center of the sphere (*i* or *j*) and the contact point. Notice that if the inner core of one sphere overlaps with external mortar layer of the other, the volume of the overlapped inner core must be discounted from the $V_{\mathrm{u,s-s}}$ and $V_{\mathrm{u,s-w}}$ obtained.

$$V_{u,s-s} = \frac{\pi}{3} \cdot \left[\left(2 \cdot {R_{T,i}}^3 - 3 \cdot {R_{T,i}}^2 \cdot d_i + {d_i}^3 \right) + \left(2 \cdot {R_{T,j}}^3 - 3 \cdot {R_{T,j}}^2 \cdot d_j + {d_j}^3 \right) \right] \quad (3)$$

$$V_{u,s-w} = \frac{\pi}{3} \cdot \left(2 \cdot {R_T}^3 - 3 \cdot {R_T}^2 \cdot d + d^3 \right) \quad (4)$$

4.3. New constructive model

In the DEM, the relative movement between particles or between particle and the wall might occur in the normal and in the tangential directions. Therefore, it is necessary to establish a rheological constitutive model that represents the behavior of the contact in both directions for the bi-phasic particle proposed.

4.3.1. Normal Direction

Studies from other authors [16-20] showed that the motion of the fresh pervious concrete in the normal direction has elastic and viscous components working simultaneously. The Kelvin-Voigt rheological model is generally used to represent this condition. This model is composed by an ideal spring arranged in parallel to a dashpot. The spring accounts for the elastic behavior of the mortar whereas the dashpot accounts for the effect of its viscosity.

Despite the widespread use, the Kelvin-Voigt rheological model induces some inconsistencies when applied to pervious concrete. Consider, for instance, two particles in contact at one point of their surrounding paste layer. When external forces are applied to approximate both particles, a rearrangement of the paste takes place around the contact point. If after a certain displacement the external forces are eliminated, the elastic part of the overlap is recovered whereas the inelastic part is maintained. The latter is the result of the viscous behavior of the dry paste that is not capable of assuming the original position once the forces are eliminated, leaving a permanent overlap.

Conversely, the Kelvin-Voigt rheological model does not allow permanent overlaps if subjected to the same loading procedure. Even though it may provide reasonable trends for the approximation stage, the same is not observed when the external loads are eliminated. The existing overlap generates an internal force induced by the compressed spring. Such force acts over the dumper connected in parallel to it, producing the gradual recovery of the overlap. Although the displacement reduces the overlap and the internal force of the spring, the remaining force leads to further displacement of the dumper. This process should continue until the force of the springs becomes 0, which will only occur when the whole overlap is recovered.

The behavior described in the previous paragraph highlights another underlying inconsistency of the Kelvin-Voigt rheological model when applied to pervious concrete. Notice that the recovery of the elastic part of the overlap is influenced by the dumper, which regulates the release of the spring. In other words, the recovery of the elastic overlap would not be instantaneous as expected in the case of a dry cement paste.

In order to solve these conceptual inconsistencies and reproduce with bigger accuracy the interaction between particles found in pervious concrete, the new contact model depicted in Fig. 8a is proposed. It is composed by a Kelvin-Voigt rheological model placed in line with a spring and a dumper, in a setup better known as Burger's model.

In this proposal, the Kelvin-Voigt rheological model accounts for the unbalanced forces that might exist in the interaction once the applied force varies over time. On the other hand, the additional spring is responsible for the instantaneous elastic recovery and the additional dumper is responsible for the inelastic part of the overlap. A contact element is also included in the representation from Fig. 8a to account for the fact that, due to the dry nature of the cement paste, breakage of contact might occur when particles are separate by a certain distance.

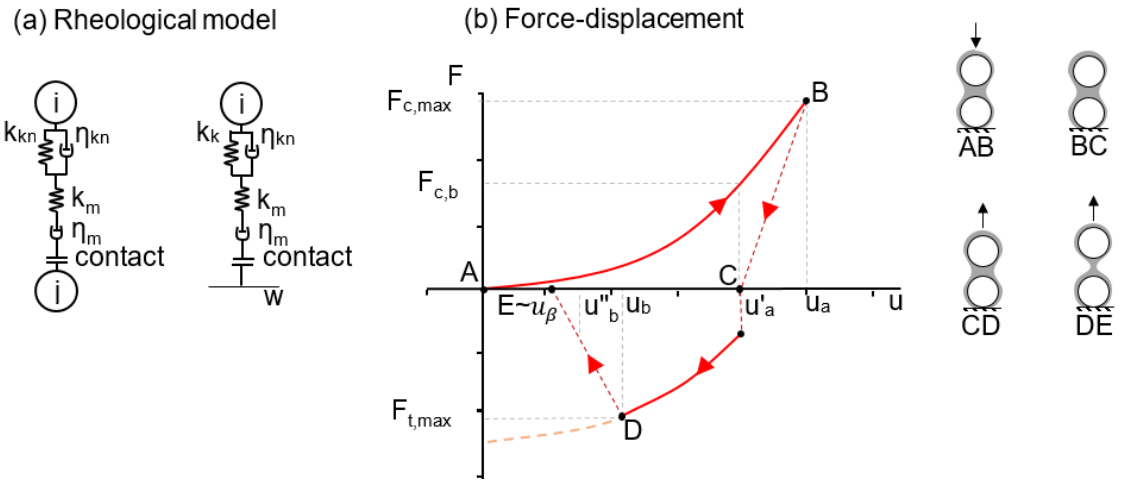

Figure 8 – Force-displacement constitutive law for an external layer contact in normal direction.

Suppose now that two particles are put in contact and an external normal force produces an overlap u with a velocity of penetration over time of $\dot{u}$. It is easy to demonstrate that, according with the rheological model of Fig. 8a, the internal normal force (F^t) generated in this contact may be calculated with Eq. 5. In this equation, Δu is the difference between the total overlap deformation (u^t) at time t and the total overlap deformation from the previous time step (u^{t-1}), u_K^{t-1} is the overlap corresponding to Kelvin-Voigt part of the model (defined by Eq. 6) and F^{t-1} is the force in the previous time step. The parameters A, B, C and D are defined in Eq. 7 to 10. k_{kn} and η_{kn} are the binder elastic coefficient and viscous coefficient for the Kelvin-Voigt part, respectively. k_{mn} is the binder elastic coefficient of the additional spring, whereas η_{mn} is the binder viscous coefficient for the additional damper.

$$F^t = \frac{1}{A} \cdot \left[\Delta u + u_K^{t-1} \left(1 - \frac{B}{C} \right) - D \cdot F^{t-1} \right] \tag{5}$$

$$u_K^t = \frac{1}{C} \cdot \left[A \cdot u_K^{t-1} + \frac{\Delta t}{2 \cdot \eta_{kn}} \cdot (F^{t-1} + F^t) \right] \tag{6}$$

$$A = \frac{\Delta t}{2 \cdot \eta_{kn} \cdot B} + \frac{1}{k_{mn}} + \frac{\Delta t}{2 \cdot \eta_{mn}} \tag{7}$$

$$B = 1 - \frac{k_{kn} \cdot \Delta t}{2 \cdot \eta_{kn}} \tag{8}$$

$$C = 1 + \frac{k_{kn} \cdot \Delta t}{2 \cdot \eta_{kn}} \tag{9}$$

$$D = \frac{\Delta t}{2 \cdot \eta_{kn} \cdot B} - \frac{1}{k_{mn}} + \frac{\Delta t}{2 \cdot \eta_{mn}} \tag{10}$$

The stiffness of the springs and the viscosity of the dampers should be closely related with the total volume of paste displaced in the contact at a certain time step ($V_{\mathrm{u,s-s}}$ or $V_{\mathrm{u,s-w}}$). It is reasonable to consider that bigger overlapped volumes would imply higher values for these parameters given that any increment on the overlap would lead to the displacement of a bigger paste volume. To simplify this consideration, it is assumed that the stiffness and the viscosity parameters may be obtained by multiplying the total overlapped volume and a base coefficient that depends solely on the rheological properties of the surrounding paste. This is represented mathematically in Eq. 11 to 14. The force-displacement curve obtained when compressive forces are applied in Eq. 5 is depicted as the curve AB in Fig. 8b.

$$k_{kn} = \begin{cases} \forall\ s-s\ : V_{u,s-s} \cdot B_{k,kn} \\ \forall\ s-w\ : V_{u,s-w} \cdot B_{k,kn} \end{cases} \tag{11}$$

$$\eta_{kn} = \begin{cases} \forall\ s-s\ : V_{u,s-s} \cdot B_{\eta,kn} \\ \forall\ s-w\ : V_{u,s-w} \cdot B_{\eta,kn} \end{cases} \tag{12}$$

$$k_{mn} = \begin{cases} \forall\ s-s : V_{u,s-s} \cdot B_{k,mn} \\ \forall\ s-w : V_{u,s-w} \cdot B_{k,mn} \end{cases} \tag{13}$$

$$\eta_{mn} = \begin{cases} \forall\ s-s : V_{u,s-s} \cdot B_{\eta,mn} \\ \forall\ s-w : V_{u,s-w} \cdot B_{\eta,mn} \end{cases} \tag{14}$$

The constitutive model proposed considers that the unloading path after an initial compression may be approximated through a straight line extending from the last point of the curve and a point in the x-axis defined by the product of the maximum displacement reached and a parameter α (curve BC in Fig. 8b). This parameter determines the level of inelastic deformation experienced by the contact, which will depend on the characteristics

of the binder. An α equal to 0 indicates that all deformation is inelastic, not being recovered. On the contrary, for higher values of α, part of the deformation is recovered.

If tensile forces are applied after the unloading stage is finished, the paste layer should deform so that the particles would start to separate from each other, as depicted by curve CD in Fig. 8b. This separation takes place according with Eq. 5 until a yielding tensile force ($F_{t,max}$) is reached. Once this occurs, the paste starts to flow around the aggregates and a striction of the meniscus takes place, causing an increase in the separation of the particles with a reduction of the tensile force applied (line DE in Fig. 8b).

The value of $F_{t,max}$ depends on the level of overlap and the load applied in the compressive stage ($F_{c,max}$). Higher absolute values of $F_{c,max}$ will lead to a bigger overlap and, consequently, bigger $F_{t,max}$. For that reason, Eq. 15 is proposed to estimate $F_{t,max}$. This equation considers that $F_{t,max}$ is obtained by multiplying $F_{c,max}$ by the proportionality constant ψ.

$$F_{t,max} = -\psi \cdot F_{c,max} \tag{15}$$

For the striction part of the diagram (CD), the stress-displacement relation is described as a straight line. This line starts at the point where $F_{t,max}$ occurs and extends over a distance that is proportional to the reduction of overlap ($u_b - u'_a$) experienced due to the tensile forces. The theoretical point u_β in which the striction curve crosses the x-axis is obtained through Eq. 16.

$$u_\beta[0-1] = \frac{(0.8-\beta)\cdot u_b}{0.8} \tag{16}$$

Fig. 9a shows an example of the constitutive law obtained with α equal to 0, ψ equal to 0.5 and β equal to 0.8. Fig. 9b shows the evolution of forces over time. Fig. 9c presents the evolution of elastics (k_{kn} and k_{mn}) and viscous (η_{kn} and η_{mn}) coefficients over time.

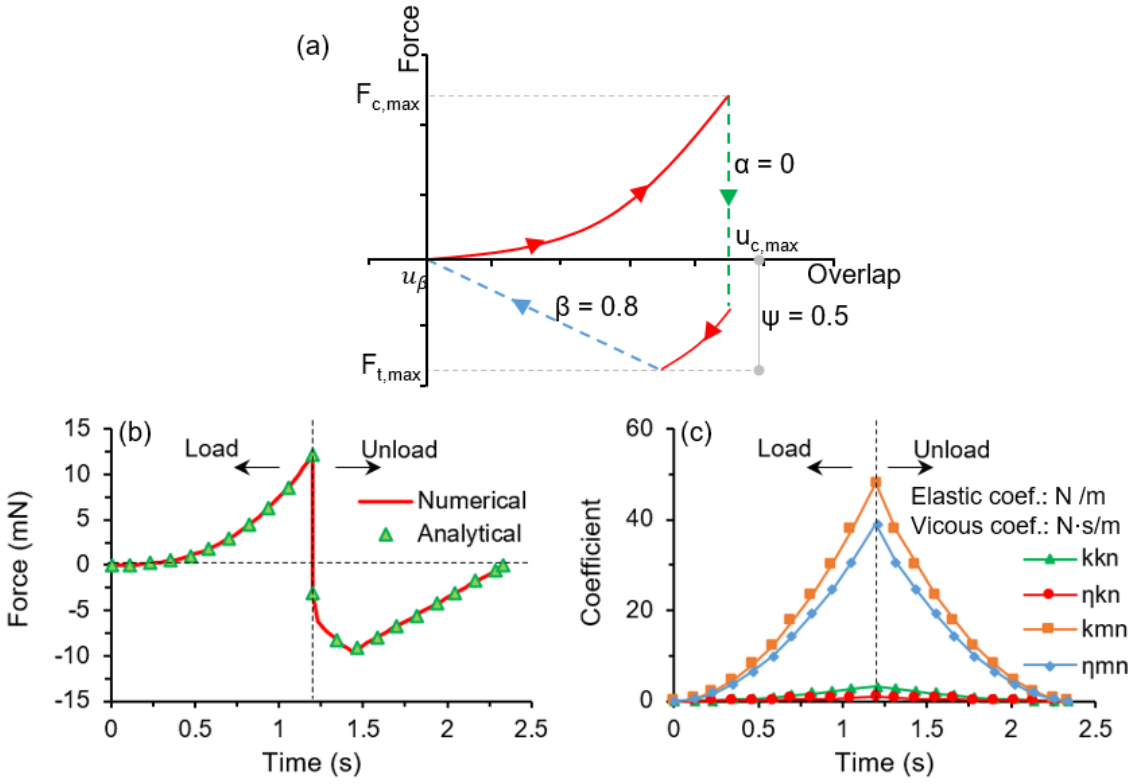

Figure 9 – Example of a force-displacement relation (a), variation of force (b) and coefficients (c) over time.

Another type of interaction occurs when the inner cores of the particles get in contact. This will happen whenever the overlap is bigger than the summed thickness of the external layer around the two particles. An analogues situation may also be found in the contact between a particle and then wall. When the overlap is bigger than the thickness of the external layer, a direct contact is established between the particle and the wall. The

rheological model used to represent both interactions is a spring in parallel with a contact element, as depicted in the Fig. 10a.

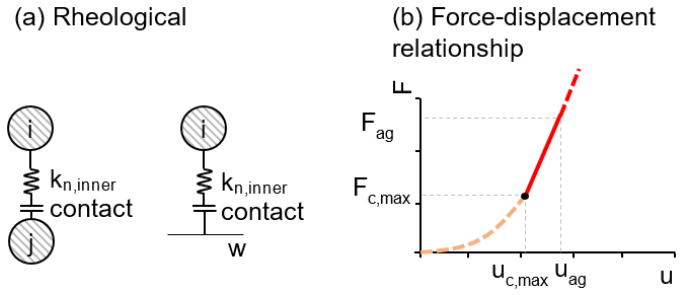

Figure 10 – Force-displacement relationship for a direct contact between the inner cores in normal direction.

The stiffness coefficient of the interaction in this case should be considerably bigger than that of the contact between the external layers. Fig. 10b shows an example of the complete force-overlap curve for two particles put in contact. It is assumed that the maximum overlap of the external layers (before the contact of the inner cores is established) is equal to '$u_{c,max}$'. For overlaps bigger than this value, the direct contact between the inner cores take place. Eq. 17 represents this relationship for overlaps bigger than $u_{c,max}$.

$$F^t = F_{c,max} + k_{n,inner} \cdot \left(u^t - u_{c,max}\right) \tag{17}$$

4.3.2. Tangential Direction

The constitutive models presented so far depend only on the overlap in the normal direction. In the case of the behavior in the tangential directions, a combined effect between the normal movement and tangential movement takes place. This is assumed because the tangential forces are affected by the normal forces acting in the contact.

The material model in the tangential direction selected is the Bingham-Hooke model, depicted in Fig 11a. The contact element responsible of identifying the contact between particles or particle and wall, is placed in series with a Bingham-Hooke model. The characteristic of the tangential motion is shear displacement in the corresponding time step, in contrast to the distance between particles in the case of normal direction. Fig. 11b shows schematically the force-displacement relationship for the interaction in the tangential direction.

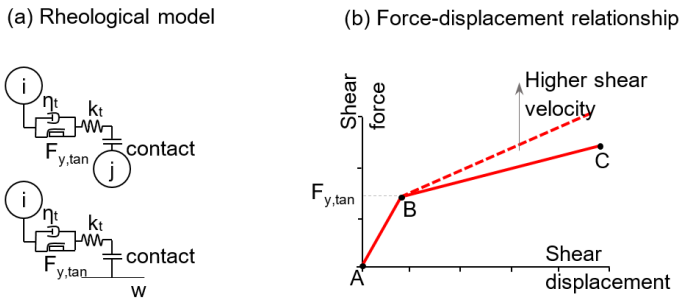

Figure 11 – Force-displacement relationship in tangential direction.

The resulting force of the tangential motion 'F_{tan}' consists of two components: elastic and viscous. The elastic component 'k_t' of the contact force depends on the tangential displacement 'u_{tan}'. The viscous component 'η_t' of the contact force is velocity-dependent and proportional to the velocity '$\dot{u}_{tan}$' of tangential motion. The force-displacement relation may be divided into two parts. The first part (represented in the Fig. 11b as the straight line AB) is elastic with small displacements, which represents the yield stress behavior. It is assumed that the deformation is small with a shear force that increases steeply, as expressed in the Eq. 18a.

Once the tangential yield force '$F_{y,tan}$' is surpassed, the rate of tangential displacement should increases, as observed in any Bingham-like fluid. To reproduce this behavior in the constitutive model, a 'slip-condition' (or 'shear cohesion') element is placed in parallel to the dumper. The resulting movement once '$F_{y,tan}$' is surpassed

corresponds to the BC line in the force–displacement relation of Fig. 12b. This is mathematically represented through Eq. 18b.

$$\begin{cases} \forall\, F_{tan} < F_{y,tan} :\ F_{tan} = k_t \cdot u_{tan} & \text{(18a)} \\ \forall\, F_{tan} \geq F_y \rightarrow\ F_{tan} = F_{y,tan} + \eta_t \cdot \dot{u}_{tan} - \dfrac{\eta_t}{k_t} \cdot \dot{u}_{tan} & \text{(18b)} \end{cases}$$

For simplification reasons, k_t and η_t are related to harmonic average of the elastics and viscous coefficients defined for the normal direction through Eq. 19 and Eq. 20, respectively. The constitutive model in the tangential direction applies for the contact between the paste layer of two particles or the direct contact of the inner cores. The only difference between these two scenarios is the friction coefficient assumed.

$$k_t = \frac{k_{kn} \cdot k_{mn}}{(k_{kn} + k_{mn}) \cdot (1 + \upsilon)} \tag{19}$$

$$\eta_t = \frac{\eta_{kn} \cdot \eta_{mn}}{(\eta_{kn} + \eta_{mn}) \cdot (1 + \upsilon)} \tag{20}$$

5. CALIBRATION WITH RESULTS FROM SHYSHKO *et al.* [21]

The parameters related to the elastics and viscous components of the normal force need calibration. This calibration was performed with the experimental results presented by Shyshko *et al.* [21]. This study [21] evaluated the normal interaction forces between two spheres (diameter equals 10 mm) with a viscoelastic material in the middle. The cement paste presents different rheological parameters over time (known as time-dependence). This complicates the tests, generating no comparable results. To mitigate this problem, the authors [21] used an aqueous solution made of Carbopol polymer. This solution was chosen because it presents a behavior according to the Bingham model and

is not time-dependent. This solution (concentration of 0.3 % by mass of water) had a viscosity of 4.9 Pa·s and a Yield stress of 42 Pa according to the Bingham model.

During the preparation of the test, the authors put the two spheres in contact. Then, the Carbopol solution is placed between the spheres. The test begins with an increase of the distance between spheres from the initial position, until the complete rupture of the meniscus of Carbopol polymer was observed (tensile mode). Then, the authors decreased the distance between the spheres (compression mode), until the direct contact of the spheres was observed. The same procedure was repeated considering displacement rates of 200, 100, 50, 20 and 10 mm/min.

A calibration of the new constitutive model proposed in section 4.3 was performed using the results by Shyshko *et al.* [21] for a displacement rate of 200 mm/min. The parameters derived from this calibration are summarized in Tab. 2. After that, the DEM simulations were repeated for the other velocities considering the same parameters from the calibration in order to validate the model.

Table 2 – Parameters of the constitutive model obtained with calibration.

Parameter	Value
α [-]	0
β [-]	1.333
ψ [-]	0.775
$B_{k,kn}$ [N/(m·m^3)]	5.23x10^6
$B_{\eta,kn}$ [N·s/(m·m^3)]	1.43x10^6
$B_{k,mn}$ [N/(m·m^3)]	7.60x10^7
$B_{\eta,mn}$ [N·s/(m·m^3)]	6.18x10^7

Fig. 12 presents the comparison between the experimental results by Shyshko et al. [17] and the results obtained numerically with the proposed constitutive law. Despite the

significant change in the velocity of the displacement applied in the test and the consequent modification in the load-strain curve, a good fit is obtained between the model and the experiments without the need of any additional calibration of parameters. For equivalent displacements showed correlation coefficients (R2) of 0.975, 0.97, 0.936, 0.947 and 0.935 for the velocities 200, 100, 50, 20 and 10 mm/min, respectively. This confirms that the constitutive law proposed here is capable of reproducing the interaction between two particles involved by a material that simulates the cement paste.

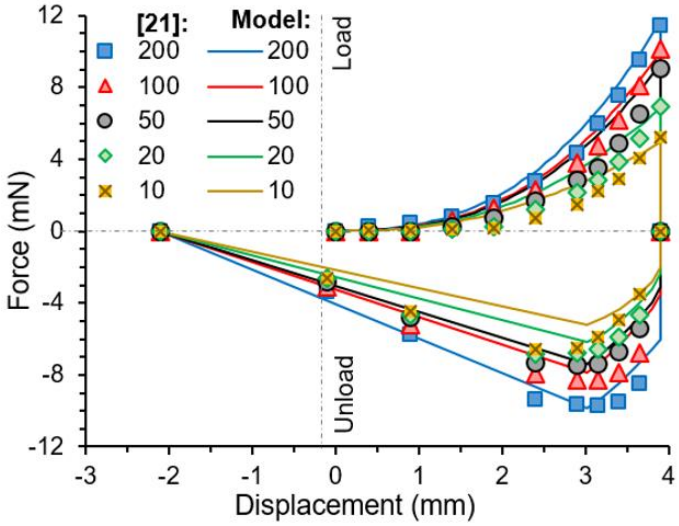

Figure 12 – Comparison of experimental results by Shyshko *et al.* [21] and results obtained from the proposed constitutive model

6. NUMERICAL SIMULATION

6.1. Simulation Process

The validations performed in the previous section accounts for a simplified interaction between two particles under highly controlled conditions. In reality, a considerably bigger number of interactions occur simultaneously, being affected by a combination of normal and tangential displacements. To evaluate the accuracy of the constitutive model proposed here in real conditions, several simulation of the tests conducted in the experimental program from section 2 were performed.

Before modeling any particle of pervious concrete, the geometry of the equipment used in the test should be modeled. This includes the mold (Fig. 13a), the funnel (Fig. 13b) and the compaction plate (Fig. 13c). All of them were modeled with facet elements. The behavior of the facets in depends on the following parameters: normal stiffness, shear stiffness, and coefficient of friction. Notice that the facet elements do not interact with each other, only with particles.

At the first stage of the simulation, the mold and the funnel are assembled as shown in Fig. 13d. The particles were then dropped inside the mold, which simulates the gravitational deposition of the particles. Once all particles are in a stable position inside the mold and the funnel, the compaction plate is generated and positioned according to the Fig. 13d. The compaction plate moves horizontally and is responsible to assure the separation between all particles above and below the height of the mold (see Fig. 13e).

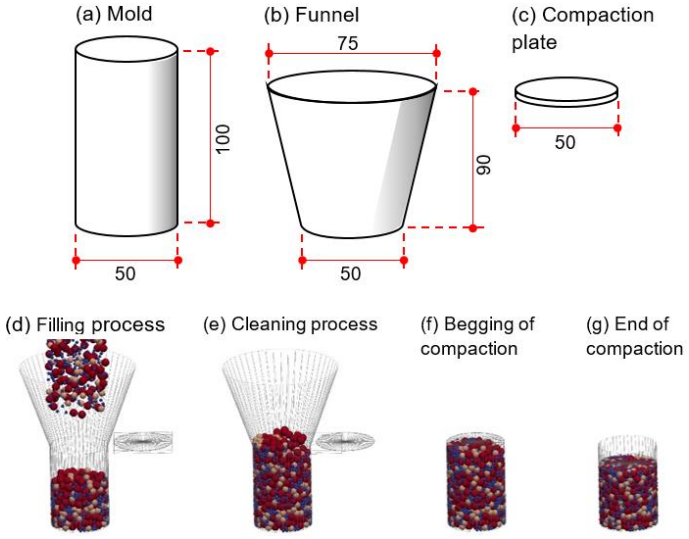

Figure 13 – Model parts (a, b and c) and simulation process (d, e, f and g)

Then, the funnel and the particles above the compaction plate are deleted, guaranteeing that all models present the same initial height. Just the particles inside the mold, the mold and the compaction plate are used in the next stage of the simulation. The

plate descends, thus producing a uniaxial compaction of the sample. Fig. 13c presents the sample with no compaction and Fig. 13d presents the sample at the end of the simulation.

Fig. 14 presents the step by step flowchart of the solution process applied during the compaction process. At the begging of each time step, the code detects all the entities with real interactions (both s-s and s-w interaction). The force and displacement are calculated for each interaction separately. The centers and radius of the particles in contact are determined. With the geometrical parameters of the entities, the zone of interaction is verified. This verification is performed to define if the interaction occurs at the paste external layer or at the inner core of the particle. Depending on the zone of contact, the material model (see Section 4.3) used to calculate the forces in the interaction is selected.

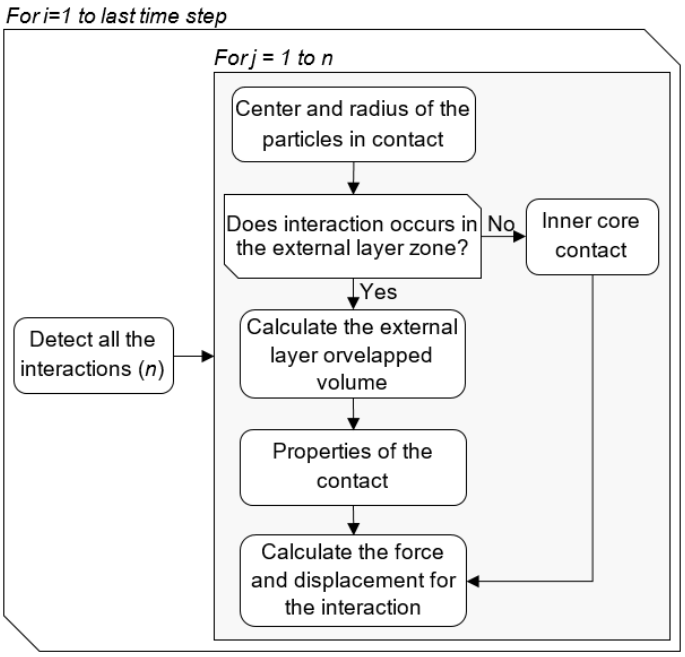

Figure 14 – Flowchart of the solution process.

In case the contact occurs at the paste external layer, the overlapped volume is calculated and the properties of the contact are assessed. Then, the forces and displacement of the entities are calculated. If the contact occurs at the inner core zone, the model represents the elastic contact and does correct the overlapped volume.

6.2. Results: Phase I

The rheology of the Carbopol polymer used by Shyshko *et al.* [21] in their experimental program to emulate the cement paste is considerably different from that of the cement paste from the experimental program conducted here. Therefore, the parameters of the constitutive model of the former should be different from those of the latter. Even though the absolute values may differ, to be consistent with previous calibrations, it is assumed that the proportion between parameters of the constitutive model is maintained regardless of the change in the rheology. In other words, a proportionality constant (K) was multiplied by all parameter from Tab. 2 in order to transform the more fluid paste of the study by Shyshko *et al.* [21] into the stiffer paste found in pervious concrete. This approach reduces the effort of calibration, since K should be the same for all tests conducted here as the w/c is 0.27 for all mixed produced.

Besides K, it is also necessary to calibrate $\alpha_{fric,e}$, $F_{y,tan}$, $k_{n,inner}$ and $\alpha_{fric,i}$. All calibrations were performed with the experimental data obtained from the compaction of family G0.22. The values obtained in this calibration are summarized in Tab. 3. Notice that the parameters obtained with the calibration using G0.22 family were used to validate the results from families G0.15, G0.17 and G0.20. The values for the distribution of the cement paste (α_{eq}) were calculated analytically according to the procedure described in Section 4.1 for each P/A and are presented in Tab. 3.

Table 3 – Parameters used in the simulation.

Parameter		**Value**
External layer	K	1000
	$\alpha_{fric,e}$	0.6
	Yield	1.0×10^6
Inner core	$k_{n,inner}$	5.5×10^{10}
	$\alpha_{fric,i}$	0.25
	$\alpha_{eq,G350}$	0.0755

Paste thickness coefficient	$\alpha_{eq,G400}$	0.0854
	$\alpha_{eq,G450}$	0.0952
	$\alpha_{eq,G500}$	0.1048

Fig. 15a shows the comparison between experimental (in gray area) stress-strain curves of the compaction process and the numerical (in straight lines) stress-strain curves obtained as the average of 5 simulations for each P/A. The shape of the numerical curve shows a first part with a low rate of increase of stress for high strain increments and the second part that presents an abrupt increase in stress for low strain increments. This agrees with the trend found in experimental results.

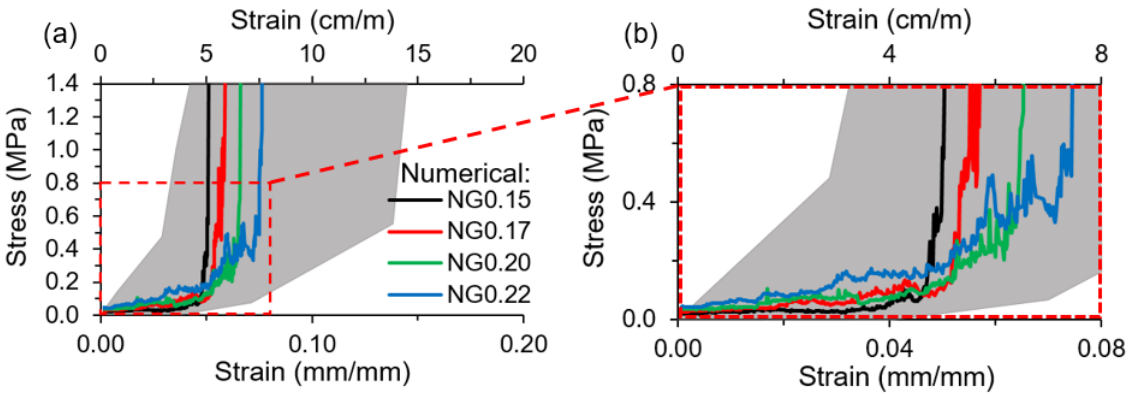

Figure 15 – Numerical and experimental results for compaction of pervious concrete made of glass spheres.

The first part of the curve is similar for all P/A ratios simulated. The strain at which the stress increases is slightly bigger for models with higher P/A. Such result is reasonable since a direct contact of the aggregates require a bigger relative displacement in mixes with a thicker layer of paste around the particles.

Despite that, the differences between the average numerical curves may be considered small in comparison with the typical scatter of the results. Consequently, the differences in the compaction curve due to the change in the P/A would be eclipsed by the scatter of the results. Again, this is consistent with the observation from the experimental program.

6.3. Results: Phase II

The same parameters from Phase I were used in the simulations of the experimental program from Phase II. The only exception is the friction between aggregates ($\alpha_{fric,i}$) that was increased to 0.75 accounting for the rougher surface of the limestone aggregates in comparison with the glass spheres. The grading curves measured in the laboratory for the aggregates were used to define the proportion and the sizes of the particles introduced in the models. The coefficient related with the thickness of the paste layer (α_{eq}) was estimated as 0.1372 according to the procedure described in Section 4.1.

Fig. 16a and 16b shows the comparison between experimental (in gray area) stress-strain curves and the numerical (in straight lines) curves obtained as the average of 3 simulations for the limestone aggregates with grading 5-12 mm and 9-20 mm, respectively. The shape of the numerical curves approximates the e. As observed during the tests, the pervious concrete with limestone aggregate of grading 5-12 mm shows a steeper increase in the stress if compared with the concrete made with coarser aggregate. Nevertheless, the influence of the grading is more pronounced in the models than in the experimental results.

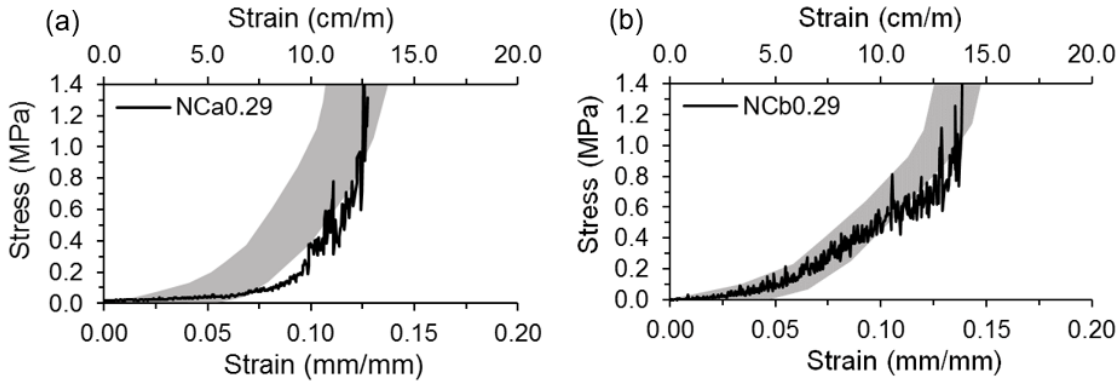

Figure 16 – Numerical and experimental results for compaction of pervious concrete made of limestone aggregates: 5-12 mm (a) and 9-20 mm (b).

Even though in general models capture the experimental behavior, differences appear in certain stretches of the stress-strain curves. In the case of the pervious concrete with limestone aggregate of grading 5-12 mm, a more abrupt increase of stress is observed. In the case of the grading 9-20 mm, small dissimilarities appear in the final part of the curve.

These differences may be caused by the simplifications regarding the shape of the particle that forms the pervious concrete. In reality, an irregular-shaped particle is used, whereas in the model all aggregates are assumed as spheres. Despite that, a good approximation of the experimental results is obtained, especially considering that the input parameters used are the same as those from Phase I. This confirms that the constitutive model proposed here combined with the simulation using DEM is capable of predicting the behavior of the material during the compaction process.

7. COMPARISON WITH THE EVOLUTIONARY LATTICE MODEL (PIERALISI *et al.* [30])

Few alternatives are available in the literature to simulate the compaction process of pervious concrete. An alternative to the approach proposed here is the Evolutionary Lattice Model (ELM) developed by Pieralisi *et al.* [30]. This has only been applied for 2D simulations of the process and assumes circular particles as well as a simplified constitutive law for the interaction between particles. To compare the accuracy of this approach and the one proposed here, a benchmark is made taking the experimental results of the pervious concrete with limestone aggregate.

The calibration of the parameters needed to simulate the compaction with the ELM [30] were performed with the experimental and numerical results obtained from the compaction of family with limestone aggregate with grading 5-12 mm. The same

parameters found in the calibration were used to validate the results with limestone aggregate with grading 9-20 mm. The elastic modulus (k_n) and the viscosity (η_n) of the cement paste were assumed 250 MPa and 200 MPa·s, respectively. The surficial stiffness (k_s) of the aggregate was set to 65 MPa/mm. The stiffness of the bars that represent the situation of no contact or virtual contact was set to approximately $1x10^{-3}$ N/mm. The value for α_{eq} used in both simulations was the same used in Section 6.3. The rate of displacement applied during the simulation was the same as during the test. Time steps of 10^{-5} s were used in all analyses.

Fig. 17a and Fig. 17b presents the numerical results with both approaches. The curve obtained with the ELM shows a slightly poorer approximation of the experimental results with the DEM and the new constitutive models. The curve of the ELM tends to present a longer stretch in the first part of the curve characterized by high strain and low stresses, achieving bigger strain levels. Conversely, it shows a stiffer behavior in the second part of the curve, characterized by an abrupt increase of the stress for small strains. This is probably the result of the simplifications of the shape and the limitations related to the movement of the particles in a 2D environment.

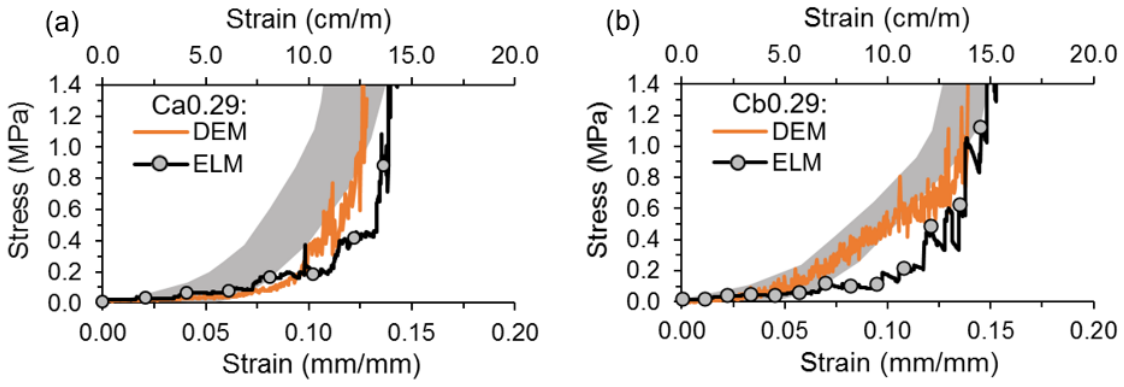

Figure 17 – Numerical comparison between the DEM and ELM [30].

The results suggest that the ELM may be used for a rough approximation of the compaction process of pervious concrete. However, if more realistic estimations are necessary, the combination of the proposed constitutive law and DEM is a better option.

8. CONCLUSIONS

The following conclusions are derived based on the numerical and experimental studies conducted in this work.

- The experimental results of the compaction of pervious concrete produced with spherical aggregates showed that the influence of the P/A over the compaction curve is negligible. The application of the numerical models proposed here explained this observation, suggesting that the small variations induced by the P/A are eclipsed by the high variability of the results.
- The experimental study of the compaction of pervious concrete in fresh state produced with crushed limestone in two different grading (5-12 mm and 9- 20 mm) showed that lower pressure was necessary to compact the specimens with bigger size of particles. This phenomenon is related to the number of contacts between aggregates, which is inversely proportional to the size of particles. The same trend was also observed in the new models developed here to simulate the compaction of pervious concrete.
- Although the Kelvin-Voigt rheological model is generally used to represent the interaction between aggregates surrounded by cement paste in fresh conventional concrete, it might lead to important inconsistencies when the contact between particles of pervious concrete is simulated. To overcome these inconsistencies, the constitutive law proposed and validated here should be used.

- The new constitutive law reproduced the normal behavior of the contact between two identical spheres with a visco-elastic material in the middle (experiments conducted by Shyshko *et al.* [21]) with accuracy. The comparison of the numerical and experimental results for equivalent displacements showed a correlation coefficient (R^2) of 0.975, 0.97, 0.936, 0.947 and 0.935 for the velocities of approximation of 200, 100, 50, 20 and 10 mm/min, respectively.
- The simulations of the compaction process of pervious concrete in fresh state showed that the proposed constitutive law is capable of reproducing the behaviors observed when pervious concrete made with aggregates with different grading curves are compacted.
- The simplifications assumed in the constitutive law regarding the simulation of the cement paste as a thin layer around the aggregate and the simulation of the aggregates as spherical particles induced small differences regarding the experimental results. Acceptable predictions were achieved, thus confirming that the DEM and the constitutive laws are suitable for the simulation of the compaction process of pervious concrete. It provides a better approximation of the phenomenon than the alternative approach available in the literature (ELM developed by Pieralisi *et al.* [30])

ACKNOWLEDGEMENTS

The corresponding author thanks the EDUCATIONAL MINISTRY OF SPAIN for the FPU Scholarship (AP2012-4188). The authors thank the companies CPV and BASF for the dedication to several research projects (especially HoPo) throughout the years. Acknowledgements are also given to the economic support provided by the Spanish

Ministry of Economy and Competitiveness to several research projects such as BIA2013-49106-C2-1-R.

REFERENCES

[1] Fresno, D.C., Bayón, J.R., Hernández, J.R., Muñoz, F.B. **Sustainable Urban Drainage Systems (SUDS)**.Interciencia. Volume 30, Issue 5, May 2005, Pages 255-260+306-308

[2] Sañudo-Fontaneda,L.A, Rodriguez-Hernandez,J., Calzada-Pérez, M.A., Castro-Fresno, D. **Infiltration behaviour of polymer-modified porous concrete and porous asphalt surfaces used in SuDS techniques.** Clean - Soil, Air, Water. Volume 42, Issue 2, February 2014, Pages 139-145. DOI: 10.1002/clen.201300156

[3] Josa, A. Jofré, C. Aguado, A. Eickschen E. y Onstenk E.. **Étude expérimentale et analyse structurelle de bétons poreux pour couches de roulement de chaussées en béton de ciment**. *Bulletin des Laboratoires des Ponts et Chaussées*, nº 208. Marzo-Abril, 1997. pp. 3-15. ISSN: 0458-5860.

[4] Pindado, M.A., Aguado, A., Josa A. **Fatigue Behavior of Polymer Modified Porous Concretes**. *Cement and Concrete Research*. Vol. 29, nº 7. July 1999, pp:1077-1083. DOI: 10.1016/S0008-8846(99)00095-2

[5] Martin, W. D., Kaye, N. B., Putman, B. J., **Impact of vertical porosity distribution on the permeability of pervious concrete.** *Construction and Building Materials*, 2014 ; 59 ; 78–84.

[6] Ibrahim, A., Mahmoud, E., Yamin, M., Patibandla, V. C., **Experimental study on Portland cement pervious concrete mechanical and hydrological properties.** *Construction and Building Materials*, 2014 ; 50 ; 524–529.

[7] Gaedicke, C., Marines, A., Miankodila, F., **A method for comparing cores and cast cylinders in virgin and recycled aggregate pervious concrete.** *Construction and Building Materials*, 2014 ; 52 ; 494–503.

[8] Gafoori, N., Dutta, S., **Laboratory Investigation of Compacted No-Fines Concrete for Paving Materials.** *Journal of Materials in Civil Engineering*, 1995 ; 7(3) ; 183–191.

[9] Suleiman, M. T., Kevern, J. T., Schaefer, V. R., Wang, K., **Effect of Compaction Energy on Pervious Concrete Properties.** *Proceedings of the 2006 NRMCA Concrete Technology Forum – Focus on Pervious Concrete*, Nashville, TN, 2006.

[10] Kevern, J. T., Schaefer, V. R., Wang, K., **Evaluation of Pervious Concrete Workability Using Gyratory Compaction.** *ASCE Journal of Materials in Civil Engineering*, 2009 ; 21(12) ; 764:770.

[11] Cundall, P. A, **A computer model for simulating progressive large-scale movements in block rock mechanics.** *Proc. Symp. Int. Soc. Rock Mech. Nancy*, 1971; 2.

[12] Cundall, P. A., Strack, O. D. L., **BALL – A program to model granular medium using the distinct element method.** *Technical Note: Advanced Technology Group*, London, 1978.

[13] Cundall, P. A., Strack, O. D. L., **A discrete numerical model for granular assemblies.** *Geotechnique*, 1979 ; 29 ; 47–65.

[14] Nabeta, K., **Flow simulation of fresh concrete by distinct element method.** *Proceedings of the Japan Concrete Institute*, 1994 ;16 ; 479-484.

[15] Chu, H., Machida, H., Suzuki, N., **Experimental investigation and DEM simulation of filling capacity of fresh concrete.** *Transactions of the Japan Concrete Institute*, 1996 ; 16 ; 9–14.

[16] Noor, U. A., Uomoto, T., **Three-dimensional discrete element method of rheology tests of self-compacting concrete.** In: *Proceeding of the First International RILEM Symposium on Self-Compacting Concrete*, Stockholm, Sweden, 1999.

[17] Puri, U., Uomoto, T., **Numerical modeling – a new tool for understanding shotcrete.** *Materials and Structures*, 1999 ; 32 ; 266-272.

[18] Chu, H., Machida, A., **Experimental evaluation and theorical simulation of self-compacting concrete by modified distinct element method (MDEM)**. In: *Recent Advances in Concrete Technology*, Fourth CANMET/ ACI/JCI International Confererence, Tokushima, Japan. 1998 ; 691-714.

[19] Zheng, J., An, X. and Huang, M., **GPU-based parallel algorithm for particle contact detection and its application in self-compacting concrete flow simulations.** *Computers & Structures*, 2012 ; 112–113 ; 193-204.

[20] Gram, A., **Numerical Modelling of Self-Compacting Concrete Flow - Discrete and Continuous Approach.** *Doctoral Thesis, Royal Institute of Technology*, 2009, Pages 66.

[21] Shyshko, S. Mechtcherine, V., **Developing a Discrete Element Model for simulating fresh concrete: Experimental investigation and modelling of interactions between discrete aggregate particles with fine mortar between them.** *Construction and Building Materials*, 2013 ; 47 ; 601-615.

[22] Mechtcherine, V., Gram, A., Krenzer, K., Schwabe, J. H., Shyshko, S., Roussel, N., **Simulation of fresh concrete flow using discrete element method (DEM): theory and applications.** *Materials and Structures*, 2014 ; 47 ; 615–630.

[23] Hoornahad, H., Koenders, E. A. B., **Simulation of macroscopic behavior of a self-compacting mixture based on DEM.** *SCC 5th North American Conference on the Design and Use of Self-Consolidating Concrete*, Chicago (USA), 2013.

[24] Mechtcherine, V., Shyshko, S., **Simulating the behaviour of fresh concrete with the Distinct Element Method – Deriving model parameters related to the yield stress.** *Cement and Concrete Composites*, 2015 ; 55 ; 81-90.

[25] Remond, S., Pizette, P., **A DEM hard-core soft-shell model for the simulation of concrete flow.** *Cement and Concrete Research*, 2014 ; 58 ; 169-178.

[26] Roussel, N., Gram, A., Cremonesi, M., Ferrara, L., Krenzer, K., Mechtcherine, V., Shyshko, S., Skocec, J., Spangenber, J., Svec, O. Thrane, L. N., Vasilic, K., **Numerical simulations of concrete flow: A benchmark comparison.** *Cement and Concrete Research*, 2015; 7.

[27] Šmilauer, V., Catalano, E., Chareyre, B., Dorofeenko, S., Duriez, J., Gladky, A., Kozicki, J., Modenese, C., Scholtès, L., Sibille, L., Stránský, J., Thoeni, K., **Yade Documentation 2nd ed. The Yade Project.** <http://yade-dem.org/doc/>.

[28] Klein, N. S., S.H.P. Cavalaro, A. Aguado, I. Segura and B. Toralles. **The wetting water in cement-based materials: modelling and experimental validation**. Accepted on Construction and Building Materials. 2016. (in press)

[29] Klein, N. S., Bachmann, J., Aguado, A., Toralles-Carbonari, B., **Evaluation of the wettability of mortar component granular materials through contact angle measurements.** *Cement and Concrete Research*, 2012; 4 (12); 1611-1620. DOI:10.1016/j.cemconres. 2012.09.001

[30] Pieralisi, R., Cavalaro, S. H. P., Aguado, A. **Evolutionary lattice model for the compaction of pervious concrete in the fresh state.** *Construction and Building Materials*, 2015, 99, 11-25. DOI:10.1016/j.conbuildmat.2015.08. 143